Engineering Failure Analysis 17 (2010) 1517–1525

Contents lists available at ScienceDirect

Engineering Failure Analysis

journal homepage: www.elsevier.com/locate/engfailanal

Investigation of high cycle and Very-High-Cycle Fatigue behaviors for a structural steel with smooth and notched specimens

Guian Qian *, Youshi Hong, Chengen Zhou

State Key Laboratory of Nonlinear Mechanics, Institute of Mechanics, Chinese Academy of Sciences, Beijing 100190, China

ARTICLE INFO

Article history:
Received 26 April 2010
Received in revised form 10 June 2010
Accepted 10 June 2010
Available online 22 June 2010

Keywords:
Very-High-Cycle Fatigue
Crack initiation
Fisheye patterns

ABSTRACT

The high cycle and Very-High-Cycle Fatigue (VHCF) properties of a structural steel with smooth and notched specimens were studied by employing a rotary bending machine with frequency of 52.5 Hz. For smooth specimens, VHCF failure did occur at fatigue cycles of 7.1×10^8 with the related *S–N* curve of stepwise tendency. Scanning Electron Microscopy (SEM) was used for the observations of the fracture surfaces. It shows that for smooth specimens the crack origination is surface mode in the failure regime of less than 10^7 cycles. While at VHCF regime, the material failed from the nonmetallic inclusion lies in the interior of material, leading to the formation of fisheye pattern. The dimensions of crack initiation region were measured and discussed with respect to the number of cycles to failure. The mechanism analysis by means of low temperature fracture technique shows that the nonmetallic inclusion in the interior of specimen tends to debond from surrounding matrix and form a crack. The crack propagates and results to the final failure. The stress intensity factor and fatigue strength were calculated to investigate the crack initiation properties. VHCF study on the notched specimens shows that the obtained *S–N* curve decreases continuously. SEM analysis reveals that multiple crack origins are dominant on specimen surface and that fatigue crack tends to initiate from the surface of the specimen. Based on the fatigue tests and observations, a model of crack initiation was used to describe the transition of fatigue initiation site from subsurface to surface for smooth and notched specimens. The model reveals the influences of load, grain size, inclusion size and surface notch on the crack initiation transition.

1. Introduction

Recently, there is a warning that fatigue failure takes place at stress levels below the conventional fatigue limit in long life regime above 10^7 cycles for high strength steels, resulting in a stepwise *S–N* curve [1–21]. In Very-High-Cycle Fatigue (VHCF) regime, crack tends to start from the interior of specimen. This fact suggests that the endurance limit determined by conventional fatigue tests cannot provide safety design data for mechanical structures. However, there is a need for a lot of mechanical structures to be used in long period, such as aircrafts, automobiles, ships, railway, bridges, etc. Therefore, there is an urgent necessity to clarify the fatigue properties and mechanism in VHCF regime.

The characteristics of crack initiation and its early growth are essential aspects in the understanding of VHCF mechanism. For the case of low cycle and high cycle fatigue, crack originates from specimen surface due to the localized plastic deformation induced by surface discontinuities. For the case of VHCF, on the other hand, cracks tend to initiate at specimen subsurface (interior). However, the process of subsurface crack initiation and propagation is still not clear and there are few

* Corresponding author.
E-mail address: qianguian@126.com (G. Qian).

1350-6307/$ - see front matter © 2010 Elsevier Ltd. All rights reserved.
doi:10.1016/j.engfailanal.2010.06.002

Nomenclature

K_t	stress concentration factor
t	notch depth
ρ	notch radius
q	fatigue notch sensitivity factor
K_f	fatigue notch factor
σ_s	fatigue strength for smooth specimens
σ_n	fatigue strength for notched specimens
σ_{max}	applied maximum stress
N_f	fatigue failure cycles
$2a$	width of fisheye
$2b$	length of fisheye
d	inclusion depth
ΔK_{inc}	stress intensity factor of nonmetallic inclusion
ΔK_{fis}	stress intensity factor of fisheye
$\sqrt{area}$	square root of the area of inclusion or fisheye
σ_a	applied stress
σ_w	fatigue strength at 10^8 cycles
HV	Vickers hardness of material
D^*	N_i/N_s
N_i	fatigue cycles required for crack initiation at subsurface
N_s	fatigue cycles required for crack initiation at surface
K	resistance of dislocation movement
k_w	the ratio of surface energy for crack formation at subsurface to that at surface
r	inclusion radius
l	grain radius
$\Delta\widetilde{U}$	dimensionless unit increment of energy
$\Delta\tau$	applied surface stress
φ	$0.5\Delta\tau/k$
ψ	r/l

theoretical models developed to analyze the different crack initiation process [8,9,13,20]. Additionally, although there have been many studies on the factors those may affect VHCF propensity of high strength steels, such as environmental medium [14–16], loading frequency [17,18], microstructure state [19–21], etc. [5,8,12], the influence of notch effect has not been fully understood.

In this paper, long term fatigue tests for a structural steel, 40Cr, were performed by a rotary bending machine operating at a frequency of 52.5 Hz. The effect of notches on the high cycle and VHCF properties was studied by introducing a circumferential notch on the specimens. After fatigue experiment tests, fracture surfaces of all specimens were examined by using Scanning Electron Microscopy (SEM) to identify the crack nucleation site. In order to understand the mechanisms of subsurface crack initiation, the notched specimens were also used to investigate the process of fatigue crack initiation and propagation by low temperature fracture technique. Based on the fatigue tests and the fracture surface observations, a model of crack initiation was used to describe the transition of fatigue initiation site from subsurface to surface for smooth and notched specimens in VHCF regime.

2. Experimental procedure

The material used in the present study is a structural steel (40Cr). The chemical compositions of the material are as follows (wt.%): C 0.4%, Cr 1% and Fe balance. The specimens were heated at 1108 K then quenched in oil, followed by tempering at 473 K for 2 h. The average Vickers hardness of the heat-treated specimen is 545Hv. The smooth specimens for fatigue testing are hour-glass type with the minimum section diameter of 3 mm as shown in Fig. 1a. The surface of the smooth specimen was sequentially polished with diamond polishing papers grits #240, #320, #400, #800 and #1200 to eliminate the surface crack. Fatigue test was conducted in cantilever-type rotating bending fatigue machines operated at the frequency of 52.5 Hz at room temperature in laboratory air. The stress ratio of the maximum to minimum load was −1. The notched specimens used for this study are also hour-glass type but with V-notch at the reduced section, as shown in Fig. 1b. The radius of notch was examined by SEM and then measured. The stress concentration factor K_t of 4.04 was calculated by the following empirical formula, according to [8].

$$K_t = 1 + 2\sqrt{\frac{t}{\rho}} = 4.04 \tag{1}$$

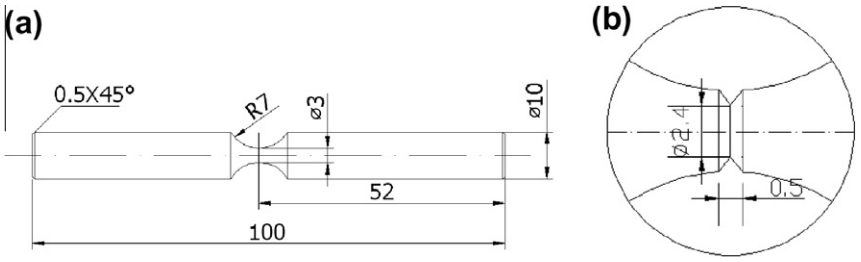

Fig. 1. Schematic of specimen (dimensions in mm). (a) Smooth specimen. (b) Notched specimen.

3. Fatigue properties

The *S–N* curves for smooth and notched specimens are shown in Fig. 2. Fatigue did occur at fatigue cycle of 7.1×10^8, which implies that it is dangerous taking conventional fatigue limit as VHCF limit. For smooth specimens, a stepwise *S–N* curve is revealed, with one representing for the surface initiated fracture and the other for the internally initiated fracture. As is seen, surface crack initiation occurred in the regime of less than 10^7 cycles, while interior crack initiation was dominant in VHCF regime. Both surface and subsurface crack initiation coexist in the plateau corresponding to 10^7 cycles. The fatigue life difference between surface crack initiation and subsurface crack initiation is due to the fact that the subsurface cracks grow in a vacuum and generally grow at an order of magnitude slower than surface initiating cracks at the same loading level. The scatter of *S–N* data is due to the large scatter in size of inclusions contained in the specimens, the variation of residual stress from compression at the surface to tension in the interior, the different surface condition, etc.

For notched specimens, a continuously decreasing curve was obtained. The maximum stress for notched specimen is the nominal stress without consideration of the stress concentration factor. For all notched specimens, fatigue crack started from the surface, which will also be shown later. For a given fatigue life, the fatigue notch sensitivity factor q was calculated by the following equation:

$$q = \frac{K_f - 1}{K_t - 1} \tag{2}$$

where K_f is defined as:

$$K_f = \frac{\sigma_s}{\sigma_n} \tag{3}$$

K_f and q at different fatigue cycles are summarized in Table 1. It is clearly that K_f and q increase with increasing of fatigue life.

4. Fractography analysis and measurement

According to SEM observations, the fatigue crack initiation site of smooth specimen could be classified into two typical modes. One is that the fatigue crack initiated on the specimen surface. Fig. 3a shows an example of surface crack initiation at

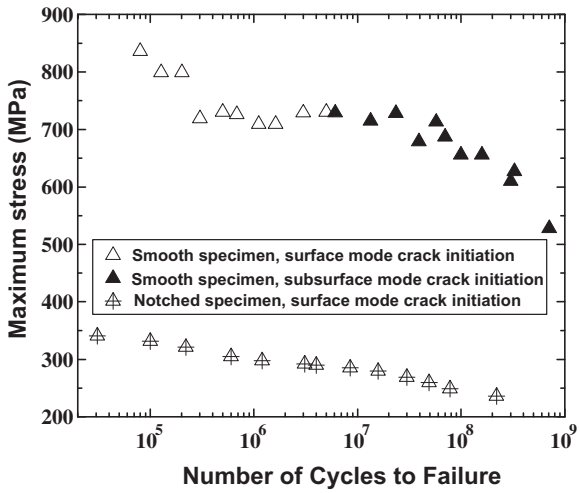

Fig. 2. *S–N* curve of 40Cr material with smooth and notched specimens.

Table 1
The fatigue sensitivity factors and fatigue notch factors at different fatigue cycles.

Fatigue life N_f	Smooth specimens		Notched specimens	
	Fatigue strength (MPa)	Fatigue strength (MPa)	K_f	q
10^5	780	335	2.33	0.44
5×10^5	735	310	2.37	0.45
10^6	725	300	2.41	0.46
5×10^6	720	291	2.47	0.48
10^7	715	282	2.53	0.50
5×10^7	700	260	2.69	0.56
10^8	658	240	2.74	0.57

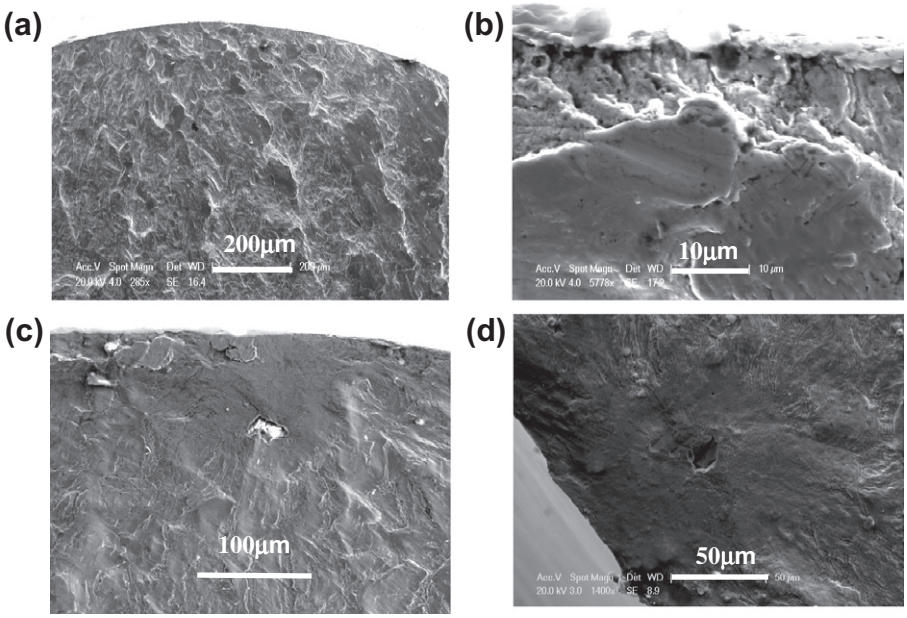

Fig. 3. SEM observations of crack initiation site for smooth specimen. (a) Specimen broke from surface. σ_{max} = 729 (MPa), $N_f = 6.09 \times 10^6$. (b) Magnification of (a). (c) Fisheye pattern. σ_{max} = 656 (MPa), $N_f = 1.59 \times 10^8$. (d) Fisheye pattern. σ_{max} = 715 (MPa), $N_f = 1.34 \times 10^7$.

failure cycle of $N_f = 6.09 \times 10^6$ and Fig. 3b magnifies the crack initiation site, which verified crack starts from surface at high stress high cycle fatigue regime. The other mode is that the fatigue crack initiated in the interior of the specimen. Fig. 3c is a typical example of a fisheye pattern, which corresponded to the failure cycle of $N_f = 1.59 \times 10^8$. A nonmetallic inclusion lies in the center of the fisheye, with the main chemical composition of Al, Si, Ca, and O. Fig. 3d shows another fisheye pattern corresponding to the failure cycle of $N_f = 1.34 \times 10^7$.

For notched specimens, it reveals that multiple crack origins are dominant on specimen surface. It is explained by the fact that the superimposed effect of the surface flaws due to the machining process and the high stress concentration factor increases the potential crack initiation sites. Fig. 4a shows the macroscopic fracture surface of a notched specimen subjected to 620 MPa, which failed at $N_f = 2.2 \times 10^8$ cycles. Fig. 4b shows the magnification of crack origins. It can be seen that all these cracks initiates from the specimen surface. They coalesce and lead to the final failure.

In order to investigate the crack initiation process, the low temperature fracture technique was used. The notched specimens were tested at the same nominal stress, σ_{max} = 240 MPa, while interrupted at different loading cycles. These survived specimens were cooled and then broken in liquid nitrogen. We checked and confirmed that the low temperature fractography of the specimen without fatigue testing is normally cleavage and quasi-cleavage morphology, as shown in Fig. 5a. Figs. 5b–d show the fracture surface of specimen which were tested up to 5×10^5, 1×10^7 and 5×10^7 respectively. Initially, the interface between inclusion and matrix is compact, as shown in Fig. 5a. It is observed that inclusion debonding appears from the loading cycles of 1×10^6, which became more evident after 1×10^7 loading cycles. Fig. 5d is an example of fractography for the specimen unloaded after 5×10^7 cycles, showing a large inclusion debonded from surrounding matrix underneath the specimen surface about 13 μm with the large fraction of fracture surface of cleavage or quasi-cleavage appearance. However, the evidence of fisheye crack was not observed on all unloaded specimens.

Figs. 6a–c are the measurements of fisheyes and the embedded inclusions from crack initiation region of the specimens. Fig. 6a shows the ratio of width to length of fisheye. It is seen that the ratio is between 0.85 and 1.15, indicating that the

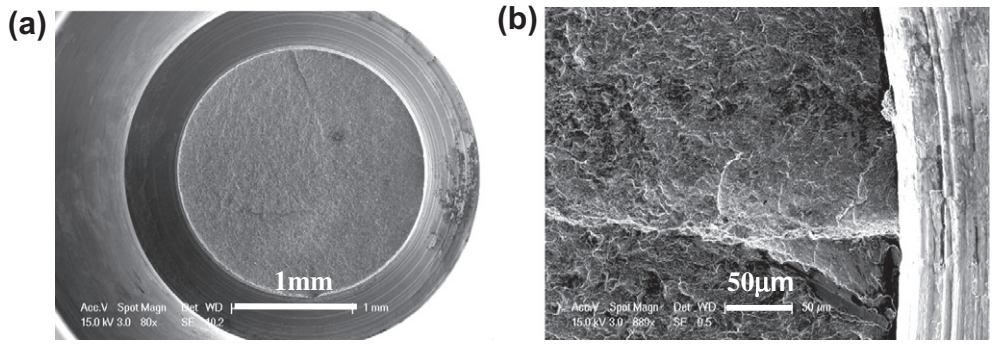

Fig. 4. SEM observations of crack initiation site for notched specimen. (a) Macroscopic fracture surface. $\sigma_{max} = 729$ (MPa), $N_f = 2.2 \times 10^8$. (b) Crack started from surface. $\sigma_{max} = 610$ (MPa), $N_f = 2.2 \times 10^8$.

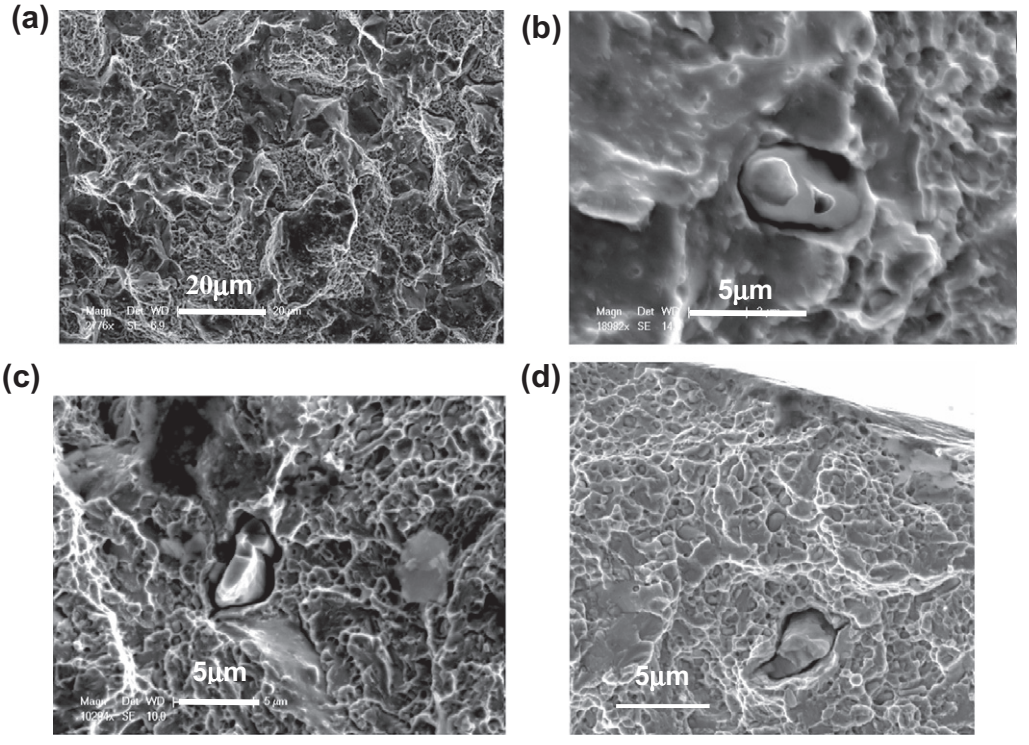

Fig. 5. SEM observations of specimens broken in liquid nitrogen. (a) $\sigma_{max} = 240$ (MPa), $N_f = 5 \times 10^6$. (b) $\sigma_{max} = 240$ (MPa), $N_f = 5 \times 10^5$. (c) $\sigma_{max} = 249$ (MPa), $N_f = 1 \times 10^7$. (d) $\sigma_{max} = 240$ (MPa), $N_f = 5 \times 10^7$.

dimension of fisheye in the direction perpendicular to specimen surface is averagely equal to that parallel to specimen surface, i.e. the shape of fisheye is almost equiaxed. Fig. 6b shows the relationship between inclusion depth and the number of cycles to failure. The distance is scattered over the range between 60 and 110 μm and increases with increasing cycles. For the inclusion which is closer to the specimen surface, less fatigue cycles are needed until the crack reaches the surface to the open air. So, with the help of air, the driving force for crack extension is larger for the crack on the surface than in the interior. In addition, according to Murakami's viewpoint [6,8], the hydrogen trapped around nonmetallic contributes to the subsurface crack initiation. It is therefore easily understood that fatigue life depends on the inclusion position. We proposed that the correlation between the fatigue life and the inclusion depth as follows:

$$N_f = 1.96 \times 10^5 d^{2.4} \tag{4}$$

Fig. 6c shows the relationship between inclusion diameter and the fatigue life. The inclusion diameter is ranged from 14 to 30 μm, which decreases with increasing of fatigue life. The tendency is in agreement with Refs. [3,7,8]. Thus, it can be seen that larger inclusions form cracks more easily than smaller inclusions.

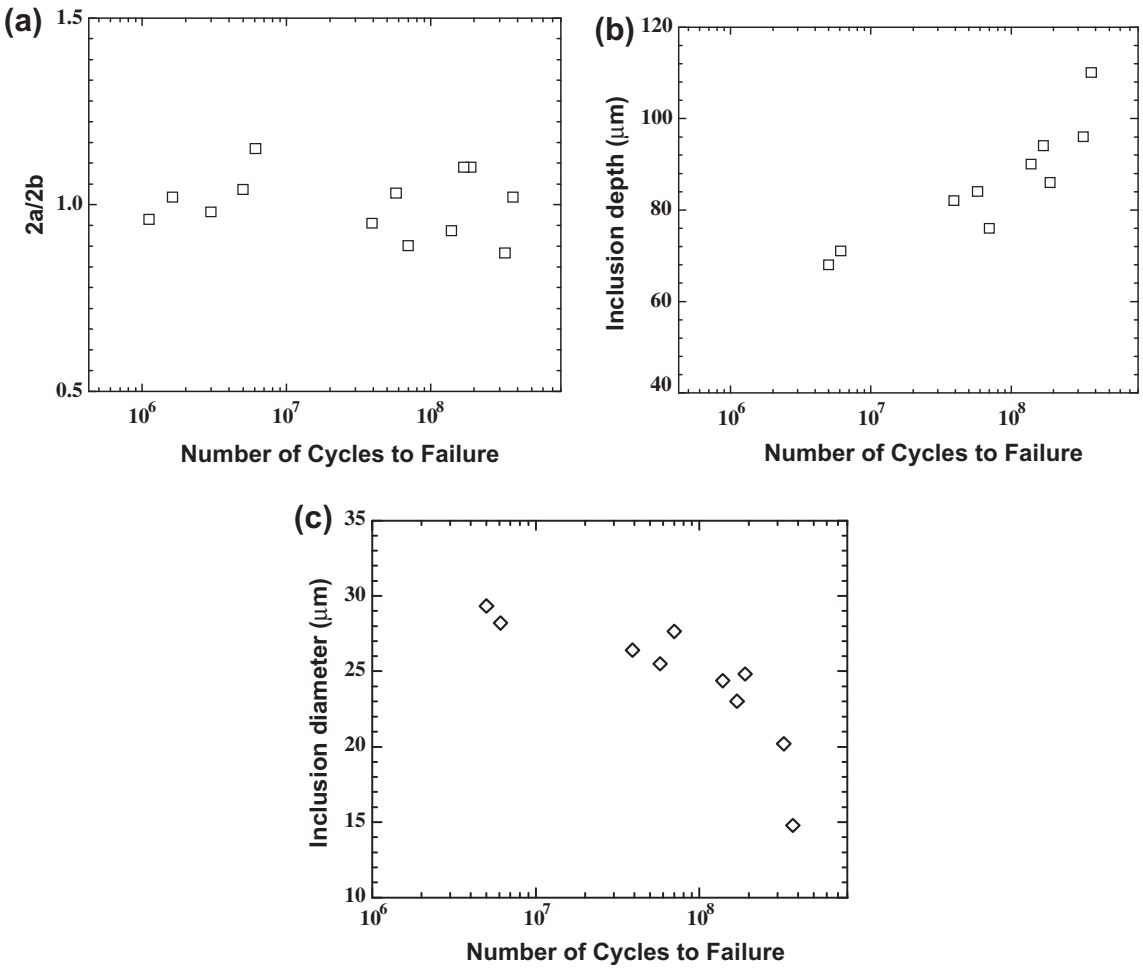

Fig. 6. Measurements of dimensions for fisheyes. (a) Relationship between $2a/2b$ and fatigue life. (b) Relationship between inclusion depth and fatigue life. (c) Relationship between inclusion diameter and fatigue life.

5. Fatigue mechanism analysis

The stress intensity factor (SIF) ranges for inclusion and fisheye pattern, i.e. ΔK_{inc} and ΔK_{fis}, were calculated by the following formula [8,22,23]:

$$\Delta K = 0.5\sigma_a\sqrt{\pi\sqrt{area}} \tag{5}$$

Fig. 7 shows the relationship between SIF ranges and number of cycles to failure. The SIF range of inclusion is about 2.83 MPa $m^{1/2}$ irrespective of the fatigue life, which is smaller than the threshold SIF range. The SIF range of fisheye is about 10 MPa $m^{1/2}$, which is corresponding to the threshold SIF range of the material. Therefore, it is understood that a crack which occurs at an inclusion can propagate below the threshold SIF range until it forms a fisheye pattern.

According to Murakami's model [5,8,22], fatigue strength at 10^8 cycles, denoted as σ_w, was predicted by the following equation:

$$\sigma_w = \frac{1.56(HV + 120)}{(\sqrt{\text{area}})^{1/6}} \tag{6}$$

Fig. 8 shows the relationship between σ_{max}/σ_w and number of cycles. The ratio is between 1 and 1.2, indicating that the fatigue strength of the material in the present study is well predicted by Murakami's model.

In order to interpret the fatigue crack initiation either at surface or at subsurface, a new parameter D^* was proposed in [24,25]:

$$D^* = \frac{N_i}{N_s} \tag{7}$$

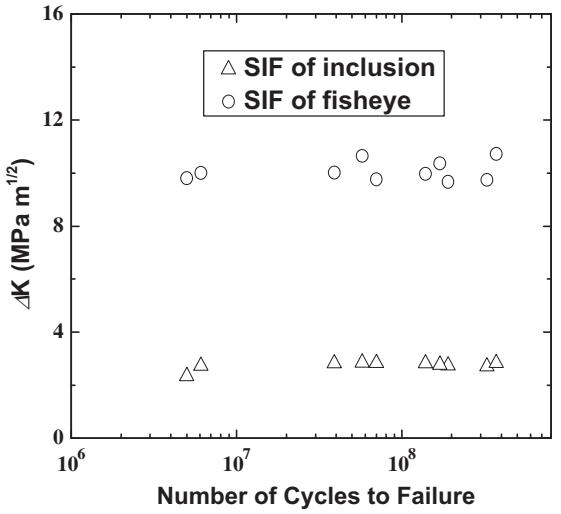

Fig. 7. SIF ranges of inclusions and fisheyes.

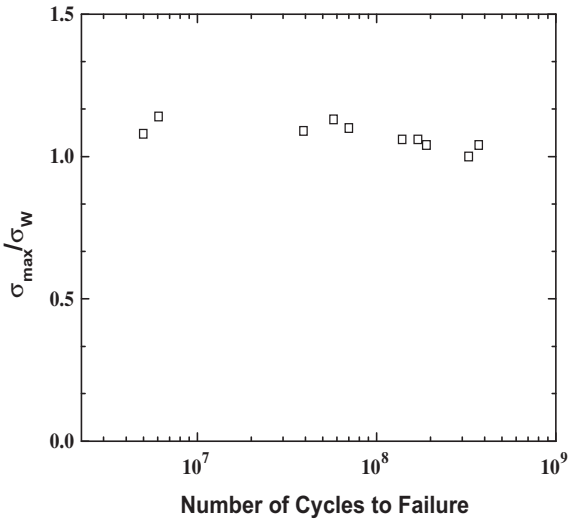

Fig. 8. Relationship between σ_{max}/σ_w and number of cycles to failure.

when $N_s < N_i$, i.e. $D^* > 1$, cracks originate at surface. On the contrary, when $N_s > N_i$, i.e. $D^* < 1$, cracks initiate at subsurface (interior).

According to the above fractographic analysis, it is noted that crack initiation from inclusions is related to the weak cohesive strength of the interface between inclusion and matrix. Under cyclic loading, a crack may easily form due to the interface debonding and grow into the matrix. For this case, it was deduced that [24,25]:

$$D^* = \frac{N_i}{N_s} = \frac{1.25k_w(\varphi - 1)^2}{\Delta\tilde{U}\psi^2} \tag{8}$$

where $\Delta\tilde{U}$ is related to φ and ψ. For notched specimens, the surface stress concentration factor is considered by the applied surface stress $\Delta\tau$. Thus, the values of D^* for both smooth and notched specimens as a function of φ and ψ were calculated and the results are shown in Fig. 9a and b, respectively.

Fig. 9a indicates that at a given loading state (φ is constant), the value of D^* increases with increasing grain size l or decreasing inclusion size r, thus crack tends to initiate at surface. With increasing ψ, i.e. the increasing inclusion size r or decreasing grain size l, the value of D^* gradually decreases and leads to $D^*<1$, then fatigue crack initiation site will shift from surface to subsurface. On the other hand, when ψ is given, the value of D^* decreases with the decreasing of φ (decrease of loading level $\Delta\tau$ or increase of dislocation resistance k, i.e. strength of material). Thus, fatigue cracks initiate at subsurface. In

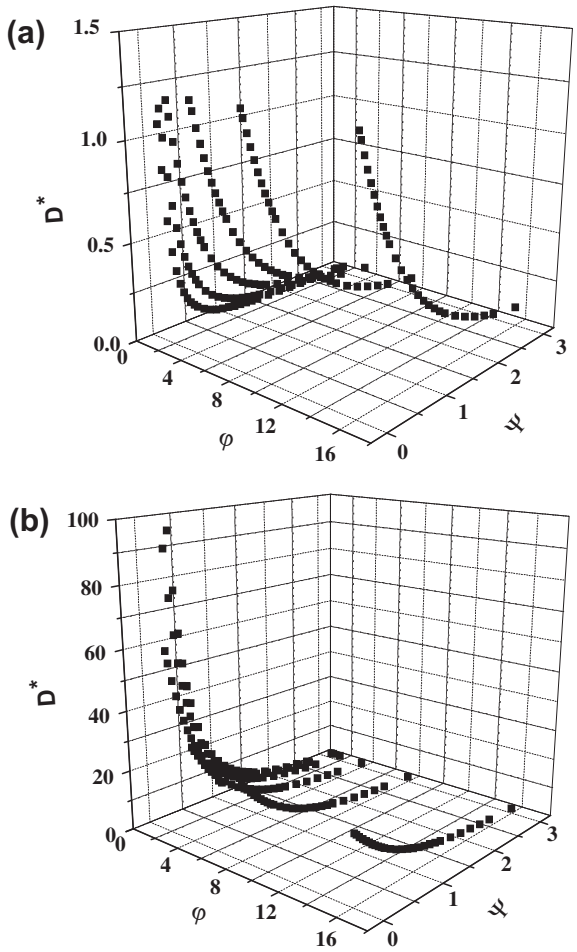

Fig. 9. Calculation results of D^* versus φ and ψ. (a) Smooth specimen. (b) Notched specimen.

other words, fatigue crack initiation tends to occur at subsurface sites at the situation of relatively low cyclic loading level, high strength of material, large inclusion size and small grain size. Therefore, it provides an insight to the material processing techniques in order to improve the fatigue life of material.

As shown in Fig. 9b, it should be noted that for notched specimens, D^* ranges from 20 to 40, which is much bigger than that of smooth specimens at the same φ and ψ. It implies that the surface crack initiation is dominant for notched specimens, which is in good agreement with the experimental observations.

6. Conclusions

Based on the fatigue tests for the low alloy steel with rotary bending fatigue machine at the cyclic frequency of 52.5 Hz, the following conclusions are drawn:

(1) VHCF failure did occur at fatigue cycles beyond 10^7 even above 10^8. For smooth specimens, the *S–N* curve is of stepwise tendency. A notable fisheye pattern was observed in the vicinity of a nonmetallic inclusion at the fracture origin in VHCF regime. The inclusion depth and inclusion size increases and decreases with increasing of fatigue life, respectively. The stress intensity factor of fisheye is relevant to the corresponding threshold of stress intensity factor. It implies that the propagation process from nonmetallic inclusion to fisheye is a process of small crack propagation.
(2) The mechanism study of fatigue crack initiation by low temperature fracture technique shows that the nonmetallic inclusion in the interior of specimen tends to debond from surrounding matrix and then to form a crack. The crack propagates and leads to the final failure.
(3) VHCF study on the notched specimens shows that the obtained *S–N* curve decreases continuously. SEM analysis reveals that multiple crack origins are dominant on specimen surface and that fatigue crack tends to initiate from the surface of the specimen.

(4) Based on the experimental observations, a model was used to describe the transition of crack initiation site with different surface conditions. At relatively low loading level, the possibility of crack initiation at subsurface increases with respect to large inclusion size, small grain size, smooth surface condition and large strength of material.

Acknowledgments

The Project was supported by the National Natural Science Foundation of China (Nos. 10772178, 10532070 and 10721202) and the Knowledge Innovation Program of the Chinese Academy of Sciences (No. KJCX2-YW-L07).

References

[1] Naito T, Ueda H, Kikuchi M. Observation of fatigue fracture surface of carburized steel. J Soc Mater Sci Jpn 1983;32:1162–6.
[2] Naito T, Ueda H, Kikuchi M. Fatigue behavior of carburized steel with internal oxides and nonmartensitic microstructure near the surface. Metall Mater Trans A 1984;15:1431–6.
[3] Shiozawa K, Lu L, Ishihara S. *S–N* curve characteristics and subsurface crack initiation behaviour in ultra-long life fatigue of a high carbon–chromium bearing steel. Fatigue Fract Eng Mater Struct 2001;24:781–90.
[4] Bathias C. There is no infinite fatigue life in metallic materials. Fatigue Fract Eng Mater Struct 1999;22:559–65.
[5] Murakami Y, Nomoto T, Ueda T. Factors influencing the mechanism of superlong fatigue failure in steels. Fatigue Fract Eng Mater Struct 1999;22:581–90.
[6] Murakami Y, Nomoto T, Ueda T, Murakami Y. On the mechanism of fatigue failure in the superlong life regime ($N > 10^7$ cycles), Part I: Influence of hydrogen trapped by inclusions. Fatigue Fract Eng Mater Struct 2000;23:893–902.
[7] Sakai T, Sato Y, Oguma N. Characteristic *S–N* properties of high-carbon–chromium-bearing steel under axial loading in long-life fatigue. Fatigue Fract Eng Mater Struct 2002;25:765–73.
[8] Murakami Y. Metal fatigue: effects of small defects and nonmetallic inclusions. Cambridge: Elsevier; 2002.
[9] Chapetti MD, Tagawa T, Miyata T. Ultra-long cycle fatigue of high-strength carbon steels. Part II: Estimation of fatigue limit for failure from internal inclusions. Mater Sci Eng A 2003;356:236–44.
[10] Shiozawa K, Morii Y, Nishino S, Lu L. Subsurface crack initiation and propagation mechanism in high-strength steel in a very high cycle fatigue regime. Int J Fatigue 2006;28:813–22.
[11] Zhou C, Qian G, Hong Y. Fractography and crack initiation of very-high-cycle fatigue for a high carbon low alloy steel. Key Eng Mater 2006;324–325:1113–6.
[12] Sakai T, Lian B, Takeda M, Shiozawa K, Oguma N, Ochi Y, et al. Statistical duplex *S–N* characteristics of high carbon chromium bearing steel in rotating bending in very high cycle regime. Int J Fatigue 2010;32:497–504.
[13] Slamecka K, Pokludaa J, Kianicovab M, Majora S, Dvorak I. Quantitative fractography of fish-eye crack formation under bending–torsion fatigue. Int J Fatigue 2010;32:921–8.
[14] Qian G, Hong Y. Effects of environmental media on high cycle and very-high-cycle fatigue behaviors of structural steel 40Cr. Acta Metall Sin 2009;45:1359–63.
[15] Nakajima M, Tokaji K, Itoga H, Ko H-N. Morphology of step-wise *S–N* curves depending on work-hardened layer and humidity in a high strength steel. Fatigue Fract Eng Mater Struct 2003;26:1113–8.
[16] Tokaji K, Ko H-N, Nakajima M, Itoga H. Effects of humidity on crack initiation mechanism and associated *S–N* characteristics in very high strength steels. Mater Sci Eng A 2003;345:197–206.
[17] Takeuchi E, Furuya Y, Nagashima N, Matsuoka S. The effect of frequency on the giga-cycle fatigue properties of a Ti–6Al–4V alloy. Fatigue Fract Eng Mater Struct 2008;31:599–605.
[18] Furuya Y, Matsuoka S, Abe T, Yamaguchi K. Gigacycle fatigue properties for high-strength low-alloy steel at 100 Hz, 600 Hz, and 20 kHz. Scripta Mater 2002;46:157–62.
[19] Ebara R. Fatigue crack initiation and propagation behavior of forging die steels. Int J Fatigue 2010;32:830–40.
[20] Gonzalo M. Dominguez Almaraz. Prediction of very high cycle fatigue failure for high strength steels, based on the inclusion geometrical properties. Mech Mater 2008;40:636–40.
[21] Krupp U, Helge K, Christ H, Koster P, Fritzen C. The significance of microstructural barriers during fatigue of a duplex steel in the high- and very-high-cycle-fatigue (HCF/VHCF) regime. Int J Fatigue 2010;32:914–20.
[22] Murakami Y, Kodama S, Konuma S. Quantitative evaluation of effects of non-metallic inclusions on fatigue strength of high strength steels. I: Basic fatigue mechanism and evaluation of correlation between the fatigue fracture stress and the size and location of non-metallic inclusions. Int J Fatigue 1989;11:291–8.
[23] Murakami Y, Usuki H. Quantitative evaluation of effects of non-metallic inclusions on fatigue strength of high strength steels. II: Fatigue limit evaluation based on statistics for extreme values of inclusion size. Int J Fatigue 1989;11:299–307.
[24] Zhou C, Experimental studies and analyses on very-high-cycle fatigue behavior of GCr15 bearing steel, Doctoral dissertation, Institute of Mechanics, Chinese Academy of Sciences; 2005 [in Chinese].
[25] Hong Y, Qian G, Zhou C, Experiment and simulation of very-high-cycle fatigue behavior for low alloy steels. In: Proceedings of 12th international conference on fracture; 2009.